Hindawi Publishing Corporation
International Journal of Chemical Engineering
Volume 2012, Article ID 786982, 13 pages
doi:10.1155/2012/786982

Research Article

Numerical Studies of the Gas-Solid Hydrodynamics at High Temperature in the Riser of a Bench-Scale Circulating Fluidized Bed

Maximilian J. Hodapp,[1] Jhon J. Ramirez-Behainne,[2] Milton Mori,[1] and Leonardo Goldstein Jr.[3]

[1] *School of Chemical Engineering, University of Campinas, 500 Albert Einstein Avenue, Campinas 13083-970, SP, Brazil*
[2] *Department of Mechanical Engineering, Federal University of Technology of Parana, Monteiro Lobato Avenue, 84016-210 Ponta Grossa, PR, Brazil*
[3] *Faculty of Mechanical Engineering, University of Campinas, 200 Mendeleyev Avenue, Campinas, 13083-970, SP, Brazil*

Correspondence should be addressed to Milton Mori, mori@feq.unicamp.br

Received 8 May 2012; Revised 3 July 2012; Accepted 10 July 2012

Academic Editor: Adrian Schumpe

The hydrodynamics of circulating fluidized beds (CFBs) is a complex phenomenon that can drastically vary depending on operational setup and geometrical configuration. A research of the literature shows that studies for the prediction of key variables in CFB systems operating at high temperature still need to be implemented aiming at applications in energy conversion, such as combustion, gasification, or fast pyrolysis of solid fuels. In this work the computational fluid dynamics (CFD) technique was used for modeling and simulation of the hydrodynamics of a preheating gas-solid flow in a cylindrical bed section. For the CFD simulations, the two-fluid approach was used to represent the gas-solid flow with the k-epsilon turbulence model being applied for the gas phase and the kinetic theory of granular flow (KTGF) for the properties of the dispersed phase. The information obtained from a semiempirical model was used to implement the initial condition of the simulation. The CFD results were in accordance with experimental data obtained from a bench-scale CFB system and from predictions of the semiempirical model. The initial condition applied in this work was shown to be a viable alternative to a more common constant solid mass flux boundary condition.

1. Introduction

Circulating fluidized bed reactors are systems in which gas-solid heterogeneous reactions take place in a fast fluidization regime. One of the most successful applications of this technology is the combustion of low-grade fuels, such as biomass, waste, and coal with high ash content. Fluidized beds provide high specific transfer rates, high solids throughput, and thermal uniformity within the reactor [1].

The total particulate material circulating in the system, the solids inventory, is an important parameter for an efficient design of CFB for combustion applications. Together with the gas superficial velocity it drives the bed particles along the loop. The pressure drop and the particle residence time are strongly related to the solid distribution in the fast bed zone (riser). Moreover, the solid distribution also affects the mass and heat transfer rates. For combustion and gasification purposes, quartz sand is commonly used as inert material due to its relatively low cost and excellent performance at high temperatures. In such systems, the amount of solid inert material can reach up to 97% of the total mass in the solids inventory [2].

Several studies have been carried out to describe the hydrodynamic behavior of the gas-solid flow in CFB systems, based on empirical and theoretical analysis at high or environmental temperatures [3–7]. The mathematical models developed sought to explain the main characteristics of the CFB system in terms of significant variables, such as

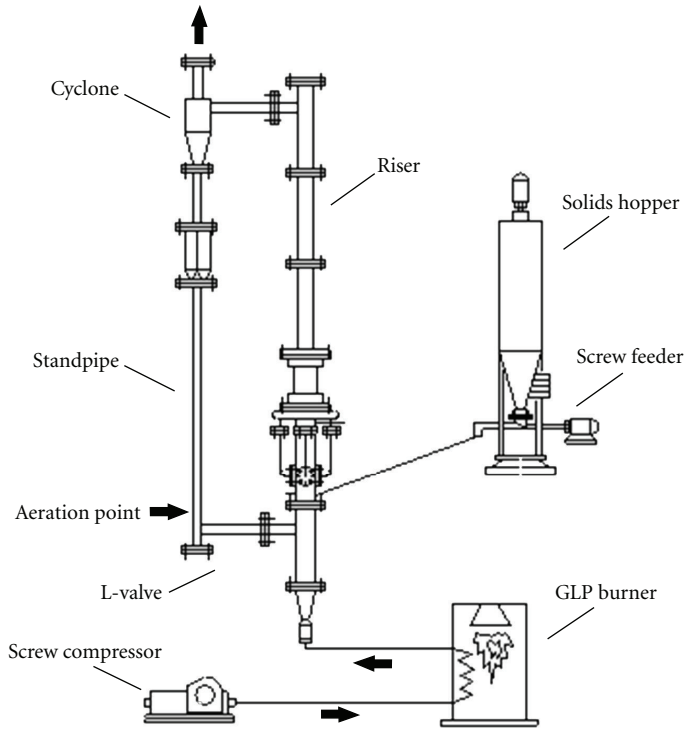

Figure 1: Experimental assembly setup, adapted from Behainne [25].

geometrical configurations, solids properties and inventory, superficial gas velocity, and solid circulation flux [8–11]. However, only a few studies reported in the literature describe a straightforward procedure to define the operational variables and geometrical measures of the components in a CFB unit for project purposes [12–14].

In a different approach to the mathematical model of CFBs, the literature has shown the successful application of the CFD technique for the simulation of many gas-solid-fluidized bed applications. Great attention has been given to the hydrodynamics in the riser component of the CFB unit. Some works have studied the behavior of FCC catalyst [15], others coal [16], and also sand particles [9].

The Eulerian-Eulerian approach is commonly applied to describe a gas-solid system. Also known as the two-fluid model, it treats the gas as well as the particulate phases as fluids, which introduces some variables that are difficult to determine for the solid phase. Thus, the kinetic theory of granular flow has been widely applied [17–19] as an analogy to the kinetic theory of gases, thereby providing closure relations for the transport equation. The two-fluid approach has been applied to different system configurations, also producing reliable results for industrial scale CFBs [20].

Cases where the available experimental data provide only the total solids inventory of the CFB loop are inappropriate for the simulation of individual components, such as risers. For the determination of initial and boundary conditions, many authors [21–23] have alternatively applied constant values for the solid mass flux entering the riser. Although this approach is valid, these are mean fluxes, not representing the variation in mass flux history over time that is observed in actual experimental units [24]. Also with a constant solid mass flux boundary condition sufficient simulation time must be computed in order to reach a pseudo-steady state, in which the actual solids inventory and thus the correct multiphase hydrodynamics are achieved in the riser. Depending on the operational and geometrical configuration, this may take too much computational effort to be viable for a tridimensional and transient CFD approach. Knowledge of the actual amount of solid material in each section of the CFB gives a further option for setting the boundary and initial conditions in the simulation of risers. Therefore the aim of this work was to use a semiempirical model to determine the required solids inventory information and verify the validity of an alternative solid reflux boundary condition.

2. Experimental Unit

A schematic view of the bench-scale CFB unit installed at University of Campinas is provided in Figure 1. The loop is composed primarily of a riser and a cyclone for solid separation, followed by a standpipe and L-valve to close the circuit.

Preheated air is supplied to the riser by a screw compressor, while the solids are fed in by a screw feeder located at the bottom of the solids hopper. Solids that are fluidized in the riser and dragged by the gas phase are collected by a tangential cyclone, which is responsible for releasing the solids into the standpipe. The L-valve controls the solid reinjection into the riser, creating a circulating system. Fine particles escaping the unit are collected by a bag filter located before the stack. Temperature measurement points are placed

Table 1: Geometrical and physical properties of the system.

Riser internal diameter, D_r	0.102 m
Standpipe/L-valve diameter, D_{lv}	0.063 m
Riser height, H	4.0 m
Particle density, ρ	2,700 kg/m^3
Particle Sauter mean diameter, d_s	353 μm
Particle specific heat, C_p	830 J/kg K
Minimum fluidization velocity[1], U_{mf}	0.06 m/s
Particle transport velocity[2], U_{tr}	5.78 m/s
Particle Geldart group	B

[1]Wen and Yu [28]; [2]Bai et al. [29].

Table 2: Operational conditions of the CFB unit.

Pressure, P	Atmospheric
Temperature, T	673 K
Fluidization velocity in riser, U	6 m/s
Total solids inventory, I	6.5 kg
Aeration mass rate at L-valve, m_a	2 kg/h

along the riser. Table 1 shows the main characteristics of the system as well as some of the physical and fluidization properties of the bed particles (quartz sand).

Yang [26] revised the particle classification of the Geldart groups for other temperatures and pressures, using the dimensionless density and the Archimedes number to determine the group divisions. Under the CFB operational conditions of the present work the solids, which were initially classified in group B under atmospheric conditions, are still considered to be on the same group.

A set of several experimental tests were conducted on this unit, as reported by Hory et al. [27]. For this study only the experimental data presented in Table 2, which represent the mean values of each variable tested in three runs, were chosen.

3. Numerical Studies

Two approaches were employed in the numerical investigation of the CFB unit, each with a specific aim. Initially a semiempirical model was assembled to determine key operational variables of a CFB system. This model was based on mathematical correlations obtained from the literature. The results produced by the semiempirical model were applied to determine boundary and initial conditions of the second approach, a CFD study of the hydrodynamics of the gas-solid flow in the unit's riser section. Both model strategies are presented in more detail as follows.

3.1. Semiempirical Model. The practical hydrodynamic model presented by Basu [2] was adapted to determine the bed solids inventory as well as other basic operational and geometrical parameters for a bench-scale CFB system. An overview of the correlations used in the semiempirical model is given in Table 3, which is divided into three stages, one for each component group of the CFB unit (riser, cyclone,

Table 3: Semiempirical CFB mathematical model.

Riser

Height (H), Kunii and Levenspiel [30]

$$\frac{\varepsilon_{g,d}-\varepsilon_{g,H}}{\varepsilon_{g,d}-\varepsilon_{g,a}}=\exp[-a(H-h_i)]$$

Decay constant, Kunii and Levenspiel [31]

$$a=\frac{4.1011\ln(d_s\cdot 10^6)-15.181}{U}$$

Choking voidage, Yang [32]

$$\frac{U_{ch}}{\varepsilon_{g,ch}}=U_{t,ns}+\sqrt{\frac{2gD\left(\varepsilon_{g,ch}^{-4.7}-1\right)\rho_s^{2.2}}{6.81\times 10^5\rho_g^{2.2}}}$$

Solids circulation flux, Yang [32]

$$G_s=(U_{ch}-U_t)\left(1-\varepsilon_{g,ch}\right)\rho_s$$

Terminal velocity of particles, Basu [2]

$$U_{t,ns}=K_{t,ns}U_t$$

where U_t and $K_{t,ns}$ are given by, Basu [2]

$$\frac{d_sU_t\rho_g}{\mu}=\frac{\mathrm{Ar}}{18}\quad \text{if Re} < 0.4$$

$$\frac{d_sU_t\rho_g}{\mu}=\left(\frac{\mathrm{Ar}}{7.5}\right)^{0.666}\quad \text{if } 0.4\le \mathrm{Re}\le 500$$

$$\frac{d_sU_t\rho_g}{\mu}=\left(\frac{\mathrm{Ar}}{0.33}\right)^{0.5}\quad \text{if } 500 < \mathrm{Re}$$

$$K_{t,ns}=0.843\log_{10}\left[\frac{\phi_s}{0.065}\right]\quad \text{if}\left\{\mathrm{Re}=\frac{d_sU_t\rho_g}{\mu}\right\}<0.2$$

$$K_{t,ns}=\left[\frac{4.89\left(\rho_s-\rho_g\right)gd_s}{3\rho_g(5.31-4.88\phi_s)}\right]^{0.5}\quad \text{if}\left\{\mathrm{Re}=\frac{d_sU_t\rho_g}{\mu}\right\}>1000$$

Superficial gas velocity, Perales et al. [33]

$$U_{tr}=U_{ch}=U=1.45\left(\frac{\mu}{\rho_gd_s}\right)\mathrm{Ar}^{0.484}$$

Axial voidage fraction, Davidson [5]

$$\left(1-\varepsilon_{g,H}\right)\rho_s=\left(\frac{E}{U}+\frac{w}{U_f}\right)$$

Internal solids reflux, Davidson [5]

$$G_s=E-\frac{R_s}{E}$$

Solids inventory, Behainne and Martins [34]

$$I_{s,r}=\left(\frac{\pi D^2\rho_s}{4}\right)\left[\left(\frac{\varepsilon_{g,H}-\varepsilon_{g,a}}{a}\right)+H\left(1-\varepsilon_{g,a}\right)-(H-h_i)\left(\varepsilon_{g,ch}-\varepsilon_{g,a}\right)\right]$$

Pressure drop, Behainne and Martins [34]

$$\Delta P_r=\frac{4gI_{s,r}}{\pi D^2}+\frac{G_s^2}{\rho_s\left(1-\varepsilon_{g,H}\right)}$$

Cyclone

Swift geometrical configuration, Basu [2]

$$A=0.44D_c;\ C=0.21D_c;\ M=0.4D_c;\ F=0.5D_c;\ S=1.4D_c;\ B=3.9D_c;\ N=0.4D_c$$

Pressure drop, Muschelknautz and Greif [35]

$$\Delta P_c=f_w\frac{A_R}{V_b}\frac{\rho_g}{2}(u_au_o)^{1.5}+\left[2+3\left(\frac{u_o}{\nu_o}\right)^{4/3}+\left(\frac{u_o}{\nu_o}\right)^2\right]\frac{\rho_g}{2}\nu_o^2$$

Wall friction coefficient, Basu [2]

$$f_w=f_0(1+2\sqrt{C_e})$$

Table 3: Continued.

Tangential gas velocity, Muschelknautz and Greif [35]

$$u_o = \frac{u_a r_o}{r_o + ((f_w/2)\ (4A_R/(\pi D^2 U))u_a\sqrt{r_a r_o}}$$

Gas exit tube radius, Muschelknautz and Greif [35]

$$u_a = \frac{u_e r_e}{r_a \alpha_1}$$

Parameters of cyclone design, Muschelknautz and Greif [35]

$$\alpha_1 = \frac{1}{\beta_1}\left[1 - \sqrt{1 - 4\left[\frac{\beta_1}{2} - \left(\frac{\beta_1}{2}\right)^2\right]\sqrt{1 - \left(\frac{1-\beta_1{}^2}{1+C_e}\right)\left(2\beta_1 - \beta_1{}^2\right)}}\right]$$

$$\beta_1 = \frac{C}{r_a}$$

Velocity at exit

$$v_o = \frac{Q}{\pi r_0^2}$$

Standpipe/solids recycle valve

Height above the aeration point, Knowlton [36]

$$L_{v,\mathrm{lv}} = \frac{\Delta P_{\mathrm{lv}} + \Delta P_{r,\mathrm{sr}} + \Delta P_c}{(\Delta P/L)_{\mathrm{mf,sp}}}$$

Pressure drop in the vertical leg of the L-valve, Knowlton [36]

$$\left(\frac{\Delta P}{L}\right)_{\mathrm{mf,sp}} = \rho_s g\left(1 - \varepsilon_{g,\mathrm{mf}}\right)$$

Pressure drop in the L-valve, Geldart and Jones [37]

$$\Delta P_{\mathrm{lv}} = 216\left(\frac{G_{s,\mathrm{lv}}^{0.17}}{D_{\mathrm{lv}}^{0.63} d_s^{0.15}}\right)$$

Pressure drop in the riser above the solids return level, Behainne and Martins [34]

$$\Delta P_{r,\mathrm{sr}} = \Delta P_r - h_{\mathrm{sr}}\left(1 - \varepsilon_{g,a}\right) g\rho_s$$

Aeration mass flow rate, Geldart and Jones [37]

$$m_{\mathrm{lv}} = m_{\mathrm{mf}}\left[\frac{(G_{s,\mathrm{lv}}/D_{\mathrm{lv}}) + 2{,}965}{3{,}354}\right]$$

Solids inventory, Behainne and Martins [34]

$$I_{s,\text{sp-lv}} = \frac{(L_{v,\mathrm{lv}} + L_{h,\mathrm{lv}})\left(1 - \varepsilon_{g,\mathrm{mf}}\right)(\pi D_{\mathrm{lv}}^2)\rho_s}{4}$$

and standpipe/solid recycle valve). The model requires input information such as riser diameter and properties of the fluidizing air and the bed particles to be initially defined. Then the solids inventory and other key conditions required for stable operation of the loop are calculated.

The total solids inventory is calculated as the sum of individual values for the riser and the standpipe/L-valve, since the particles of the CFB system are mainly concentrated in those components.

3.2. CFD Model. For a better understanding of the behavior of the gas-solid flow in the riser, a CFD study was carried out. CFD can produce detailed information on multiphase flows, which is not always readily obtained on experimental units. The gas-solid flow information produced can also be used to aid in the improvement of the system design.

The governing equations for the momentum, turbulence, and energy transport were used to describe the phenomena involved in the multiphase flow inside the riser. The gas-solid system was represented by the Eulerian-Eulerian approach,

Table 4: Hydrodynamic and thermal models for the two-fluid gas-solid flow approach.

Continuity

$$\frac{\partial}{\partial t}(\varepsilon_i \rho_i) + \nabla \cdot (\varepsilon_i \rho_i \vec{v}_i) = 0$$

Gas-phase momentum

$$\frac{\partial}{\partial t}\left(\varepsilon_g \rho_g \vec{v}_g\right) + \nabla \cdot \left(\varepsilon_g \rho_g \vec{v}_g \vec{v}_g\right) = -\varepsilon_g \nabla P_g + \nabla \vec{\tau}_g + \varepsilon_g \rho_g \vec{g} + \beta\left(\vec{v}_s - \vec{v}_g\right)$$

Gas-phase stress tensor

$$\vec{\tau}_g = \varepsilon_g \mu_g\left(\left(\nabla \vec{v}_g + \left(\nabla \vec{v}_g\right)^T\right) - \frac{2}{3}\left(\nabla \cdot \vec{v}_g\right)\vec{I}\right)$$

Solid-phase momentum

$$\frac{\partial}{\partial t}(\varepsilon_s \rho_s \vec{v}_s) + \nabla \cdot (\varepsilon_s \rho_s \vec{v}_s \vec{v}_s) = \nabla \vec{T}_s + \varepsilon_s \rho_s \vec{g} + \beta\left(\vec{v}_g - \vec{v}_s\right)$$

Solid-phase stress tensor

$$\vec{T}_s = (-P_s + \lambda_s \nabla \cdot \vec{v}_s)\vec{I} + \mu_s\left(\left(\nabla \vec{v}_s + (\nabla \vec{v}_s)^T\right) - \frac{2}{3}(\nabla \cdot \vec{v}_s)\vec{I}\right)$$

Solid-phase pressure, Ogawa et al. [38]

$$P_s^{k+t} = \rho_s \varepsilon_s [1 + 2(1+e)\varepsilon_s g_o]\ \theta$$

Particle-particle restitution coefficient, Jiradilok et al. [21]

$$e = 0.9$$

Radial distribution function, Ogawa et al. [38]

$$g_o = \left(1 - \left(\frac{\varepsilon_s}{\varepsilon_{s,\max}}\right)^{1/3}\right)^{-1}$$

Solid-phase bulk viscosity, Lun et al. [39]

$$\lambda_s = \frac{4}{3}\varepsilon_s^2 \rho_s d_s g_o (1+e)\sqrt{\frac{\theta}{\pi}}$$

Solid-phase shear viscosity, Gidaspow [17]

$$\mu_s = \frac{4}{5}\varepsilon_s \rho_s d_s g_o (1+e)\left(\frac{\theta}{\pi}\right)^{1/2} + \frac{\varepsilon_s \rho_s d_s \sqrt{\theta\pi}}{6(3-e)}\left(1 + \frac{2}{5}(1+e)(3e-1)\varepsilon_s g_o\right)$$

Gas-solid drag, Gidaspow [17]

$$\beta = 150\frac{\varepsilon_s^2 \mu_g}{\varepsilon_g d_s^2} + 1.75\frac{\left|\vec{v}_s - \vec{v}_g\right|\varepsilon_s \rho_g}{d_s} \quad \text{for } \varepsilon_g \le 0.8$$

$$\beta = \frac{3}{4}C_D\frac{\left|\vec{v}_s - \vec{v}_g\right|\varepsilon_s \rho_g}{d_s}\varepsilon_g^{-2.65} \quad \text{for } \varepsilon_g > 0.8$$

$$C_D = \frac{24}{\mathrm{Re}}\left(1 + 0.15\mathrm{Re}^{0.687}\right) \quad \text{for Re} < 1{,}000$$

$$C_D = 0.44 \quad \text{for Re} \ge 1{,}000$$

Energy balance

$$\frac{\partial}{\partial t}(\varepsilon_i \rho_i H_i) + \nabla \cdot (\varepsilon_i \rho_i \vec{v}_i H_i) = \nabla(\alpha_i \nabla T_i) + h_{ij}\left(T_i - T_j\right) + S_i$$

Heat exchange, Ranz and Marshall [40]

$$h_{ij} = \frac{6k_g \varepsilon_g \varepsilon_s \mathrm{Nu}}{d_s{}^2}$$

$$\mathrm{Nu} = 2 + 0.6\mathrm{Re}_s^{0.5}\mathrm{Pr}^{0.333}$$

which considers each phase as a fluid. For describing the turbulence in the gas phase, the realizable k-epsilon model was applied and the solid phase was modeled by the KTGF, following the general approach adopted by many authors for multiphase flow in risers. The main equations in the model are presented in Table 4.

The solid stress tensor was described through the KTGF, which accounts for the solid viscosity and pressure terms.

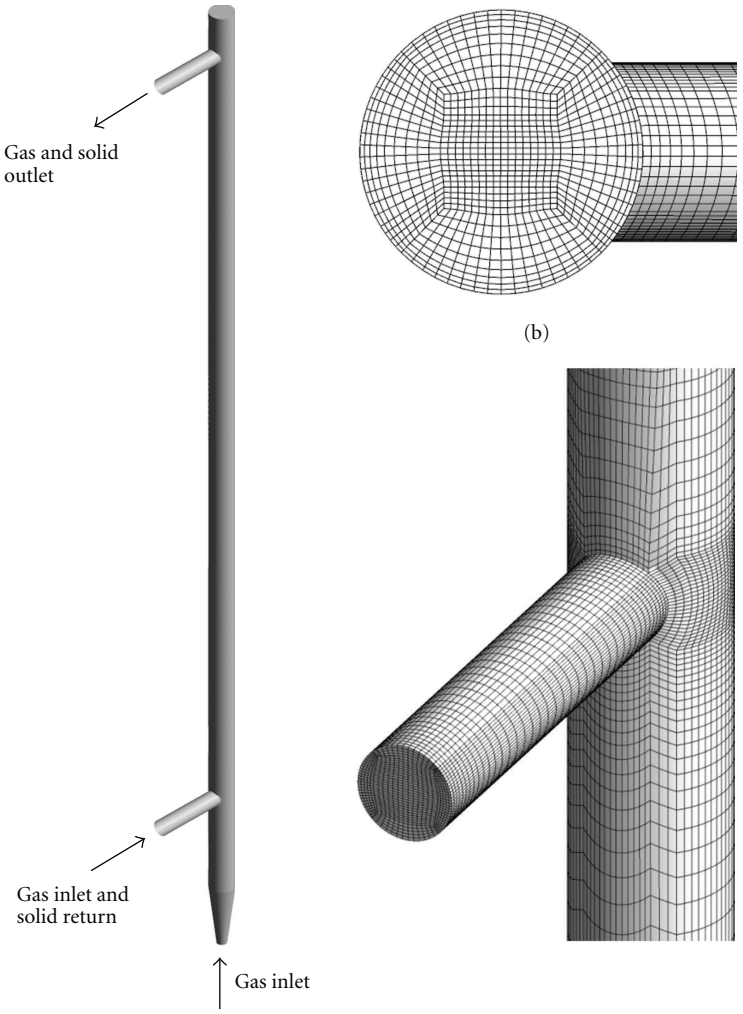

Figure 2: Details of (a) the generated geometry, (b) numerical mesh of the top section, and (c) numerical mesh of the bottom section of the riser for the CFD simulation.

Table 5: Boundary conditions for the CFD riser simulation.

	Gas phase	Solid phase
Main inlet	Mass flow rate: $2.468 \cdot 10^{-2}$ kg/s; Temperature: 900 K	
Secondary inlet	Mass flow rate: $5.56 \cdot 10^{-4}$ kg/s; Temperature: 624 K	Mass flow rate: recirculation function; Temperature: 624 K
Outlet	Pressure: 0 Pa	Pressure: 0 Pa
Walls	No slip Heat flux: -175 W/m^2	Free slip Heat flux: -175 W/m^2

Table 6: Input data used in the semiempirical model based on Hory et al. [27].

Internal diameter of the riser column, D	0.102 m
Height of the secondary air injection, h_i	0.9 m
Solids reflux ratio, R_s	0.066
Operation temperature, T_b	673 K
Operation pressure, P_b	101.3 kPa
Voidage fraction bottom region of the riser, ε_a [1]	0.9
Solid sphericity, ϕ_s [1]	0.75

[1] Values supported by Basu [2].

The granular temperature was related to the kinetic turbulent energy of the particle and the transport equation derived from it in the kinetic theory is simplified to an algebraic formulation. As for the thermal balance in the riser, a transport equation was solved for each phase. The pressure work, kinetic energy, and viscous heating were neglected as the flow occurs at low Mach numbers [16]. The heat exchange between the two phases was expressed by the Ranz and Marshall [40] correlation.

Table 7: Results obtained from the semiempirical model.

Riser	Particle terminal velocity corrected by sphericity, $U_{t,\mathrm{ns}}$	3.04 m/s
	Superficial gas velocity, $U = U_{\mathrm{tr}} = U_{\mathrm{ch}}$	5.54 m/s
	Solids circulation flux in the riser, G_s	20.93 kg/m$^2\cdot$s
	Choking voidage, $\varepsilon_{\mathrm{ch}}$	0.9969
	Voidage fraction at the riser exit, ε_H	0.9962
	Riser height, H	4.00 m
	Riser height-to-internal diameter ratio, $R_{H\text{-}D}$	39.2
	Solids inventory in the total riser height, $I_{s,r}$	3.52 kg
	Pressure drop in the total riser height, ΔP_r	4,268 Pa
	Solids return level above the riser base	0.45 m
	Pressure drop in the riser measured above the solids return level, $\Delta P_{r,\mathrm{sr}}$	3,077 Pa
Cyclone	Volumetric gas flow entering the cyclone, Q	0.045 m/s
	Solid-to-gas mass ratio at the cyclone entrance, C_e	3.8
	Gas velocity at the inlet section of the cyclone, u_e	14.83 m/s
	Cyclone dimensions [m]: Dc = 0.182; A = 0.080; C = 0.038; M = 0.073; F = 0.091; S = 0.255; B = 0.709; N = 0.073.	—
	Gas velocity at the cyclone exit, v_o	10.90 m/s
	Pressure drop in the cyclone, ΔP_c	271 Pa
Standpipe and L-valve	Internal diameter of the standpipe and the L-valve, D_{lv}	0.063 m
	Circulating solids flux in the standpipe and the L-valve, $G_{s,\mathrm{lv}}$	55.2 kg/m$^2\cdot$s
	Solids velocity in the moving bed, $U_{s,\mathrm{lv}}$	0.04 m/s
	Horizontal section of the L-valve, $L_{h,\mathrm{lv}}$	0.36 m
	Aeration level above of the horizontal section center line, L_a	0.13 m
	Aeration mass flow rate in the L-valve, m_{lv}	1.97 kg/h
	Height of the solids above the aeration point, $L_{v,\mathrm{lv}}$	0.50 m
	Height of the standpipe, L_{sp}	2.71 m
	Pressure drop in the L-valve, ΔP_{lv}	3,917 Pa
	Pressure drop in the standpipe, ΔP_{sp}	7,265 Pa
Total solids inventory in the CFB system		8.20 kg

Only the riser was considered for the CFD simulation, since this is the section of interest in most of industrial applications and where experimental data was collected for validation. This simplification also avoids extracomputational efforts for simulating the very dense regions in the L-valve, through which the solids return to the riser. A hexahedral mesh containing approximately 400 thousand control volumes was created for the riser. A set of finer and coarser mesh was also created, whereas the refinement of the one selected was sufficient for producing grid independent results for the nonisothermal multiphase flow. The mean equivalent cell length to particle diameter for the selected grid was around 37. Details of the geometry and numerical grid are shown in Figure 2.

Atmospheric air represented the continuum phase and quartz sand the dispersed phase. The boundary conditions are described in Table 5. At the main air entrance (bottom zone), a constant gas mass flow rate was specified, at the temperature measured at the exit of the GLP burner. At the secondary inlet, where the solid returns to the riser, air from the L-valve enters at a constant mass flow rate. The temperature boundary condition of the secondary entrance was determined by experimental measurements at the L-valve exit and was considered the same for both phases as they reenter the riser. A mathematical function was implemented to inject sand at the same mass flow rate as that calculated at the riser exit at each time step. In order to apply this condition it was necessary to determine the mass of sand that would be present only in the riser, since considering the total solids inventory of the entire loop would greatly overestimate the solid recirculation rate, which in turn would modify the system's fluid dynamic behavior. This information was obtained from the semiempirical model. At the walls the no-slip boundary condition was applied for the gas phase and free slip for the solid phase, a simplified but close to the correct low-friction condition for the dispersed phase, according to [19]. The heat loss to the environment was also considered as a constant negative heat flux.

In order to reproduce the behavior of the gas-solid flow in a vertical riser, transient simulations were considered. The numerical formulation followed the finite volume method by means of the commercial software Ansys Fluent 12.0. For the interpolation of the discretized partial differential equations, the first-order upwind scheme was used. The convergence

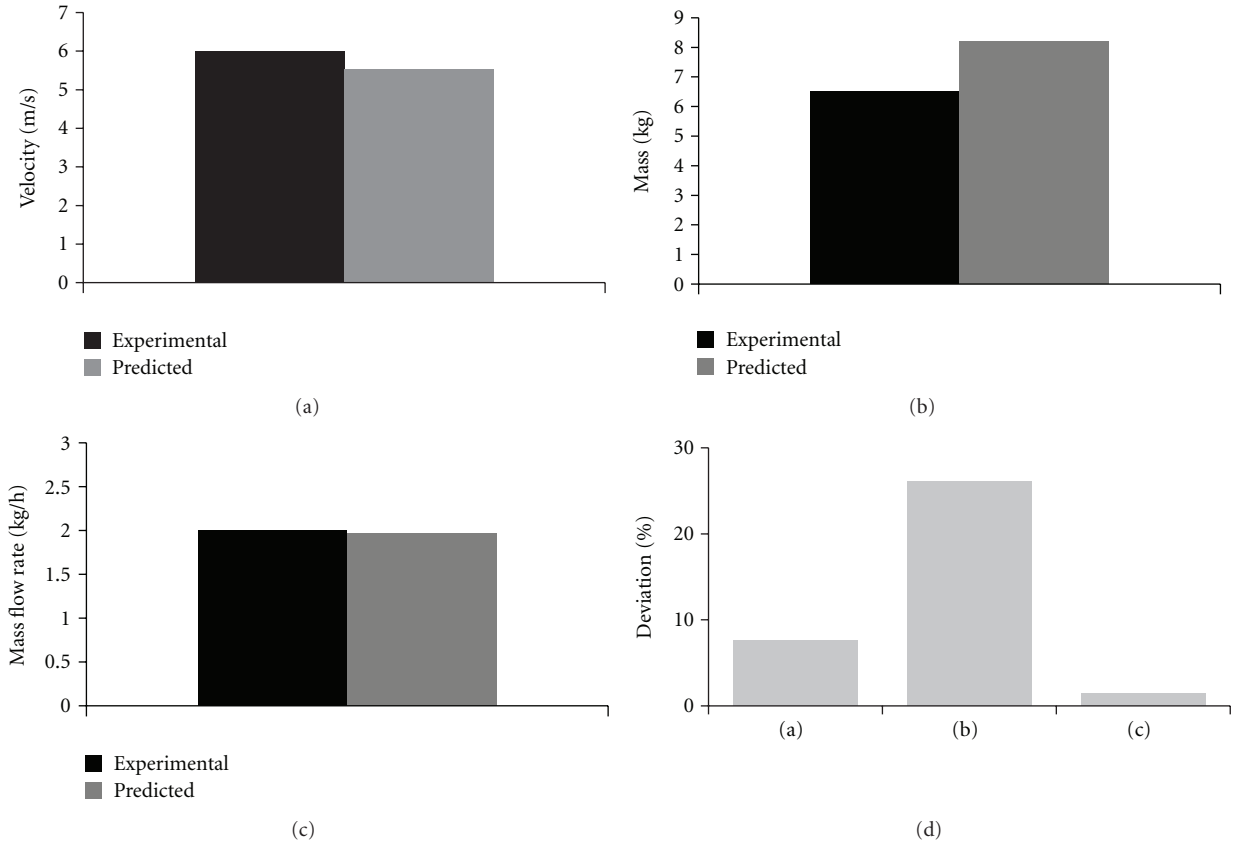

Figure 3: Comparison of the semiempirical model results for (a) superficial gas velocity (U), (b) solids inventory (I), (c) aeration mass flow rate (m_{lv}), and (d) deviation for each variable.

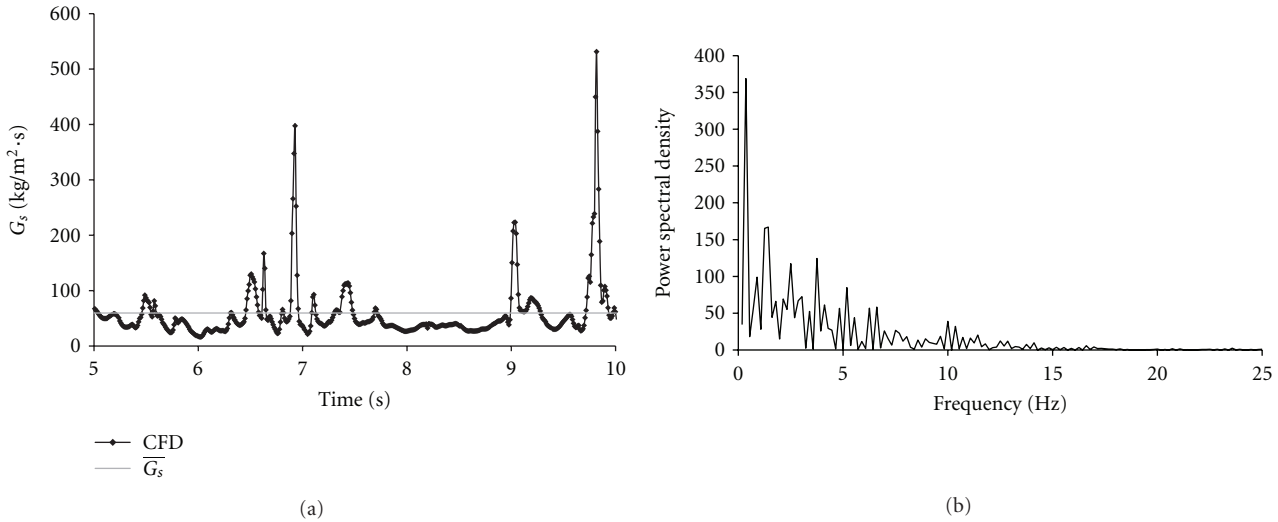

Figure 4: CFD simulation results of solid phase mass flux leaving the riser: (a) time history fluctuations and (b) power spectral density.

criterion was established as 10^{-3} in absolute values. Reduced underrelaxation factors were chosen to improve the stability of the solution. The time step of 10^{-5} s was initially adopted and gradually increased to a maximum value of 10^{-4} s.

4. Results and Discussion

As the main purpose of the semiempirical model was to ease the preliminary system setup for the CFB unit, a validation was carried out comparing its results to those obtained from

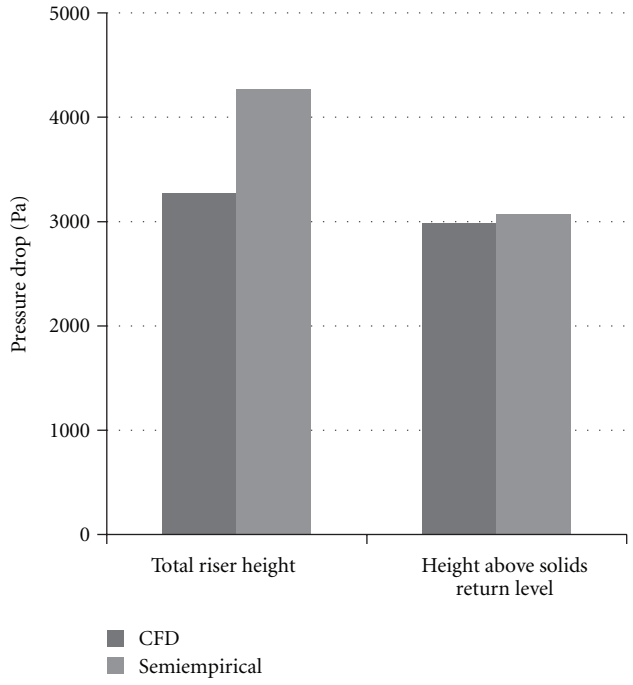

Figure 5: Pressure drop in the riser as given by the semiempirical model and the CFD simulations.

the experimental data shown in Table 2. Furthermore, the internal solids reflux ratio R_s was set at the appropriate value to guarantee the same riser height of the experimental CFB combustor. Table 6 contains the input data of the model based on the experimental unit conditions.

The results obtained from the semiempirical model for each section of the CFB unit are presented in Table 7, and the comparison with experimental data for superficial gas velocity, solids inventory, and aeration mass flow rate in L-valve is shown in Figure 3.

In Figure 3 it is shown that the predictions for U, $I_{s,T}$, and m_{lv} were consistent with the experimental values. For the total solids inventory, the result obtained in the simulation was overestimated by approximately 26%. The gas superficial velocity and the aeration rate were very close to the plant operational conditions. In general, these results are considered satisfactory for preliminary design of CFB loops.

According to these results, the amount of solids in the riser corresponds to approximately 43% of the total solids inventory. This information produced by the semiempirical model was used for setting the initial condition for the CFD simulation of the riser. Thus an initial packed bed was set at the base of the riser corresponding to the stipulated solid mass.

The simulation was carried out for 10 s, during which time a quasi-steady state was achieved. At the initial seconds of simulation, the inert bed was observed to begin a rapid fluidization, reaching the riser's exit and starting to return to the riser. Nevertheless, only after 5 seconds of simulation, transient statistics averages were collected for the main variables in order to analyze the riser characteristics.

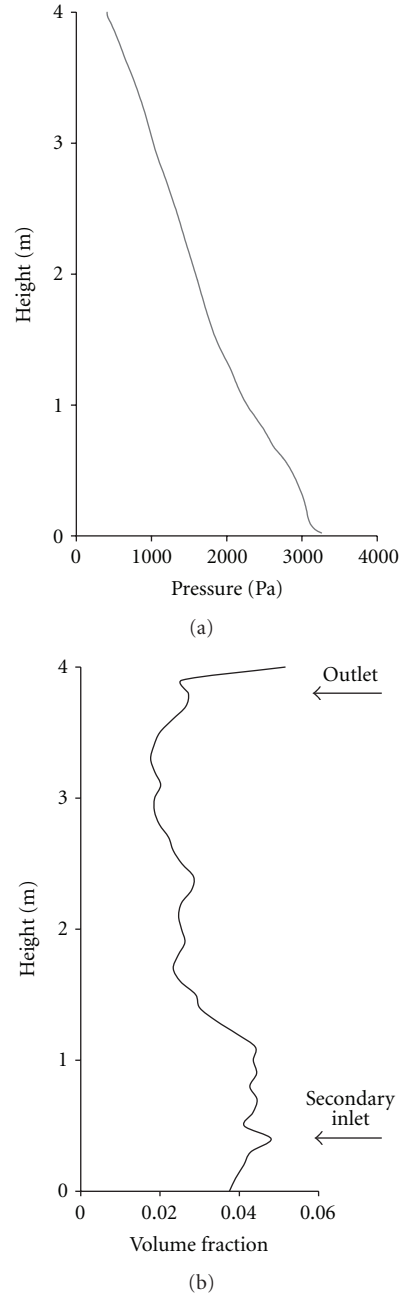

Figure 6: Time-averaged CFD axial profiles for (a) pressure at the center line and (b) solid phase volume fraction calculated as an area average at several cross section planes along the height of the riser.

The multiphase flow in fluidized beds (risers) is known for its chaotic behavior, as can be observed by the solid phase mass flux leaving the riser (Figure 4(a)). The CFD simulation captured this behavior, although the solid residence time in the cyclone and standpipe was neglected. The G_s calculated at the exit at every time step was applied to the recirculation boundary condition. The mass flux fluctuations at the recirculation entry were computed without any delay. The average solid recirculation mass flux ($\overline{G}_s$) predicted by the CFD simulation was 59 kg/m^{2}s, which agreed well with

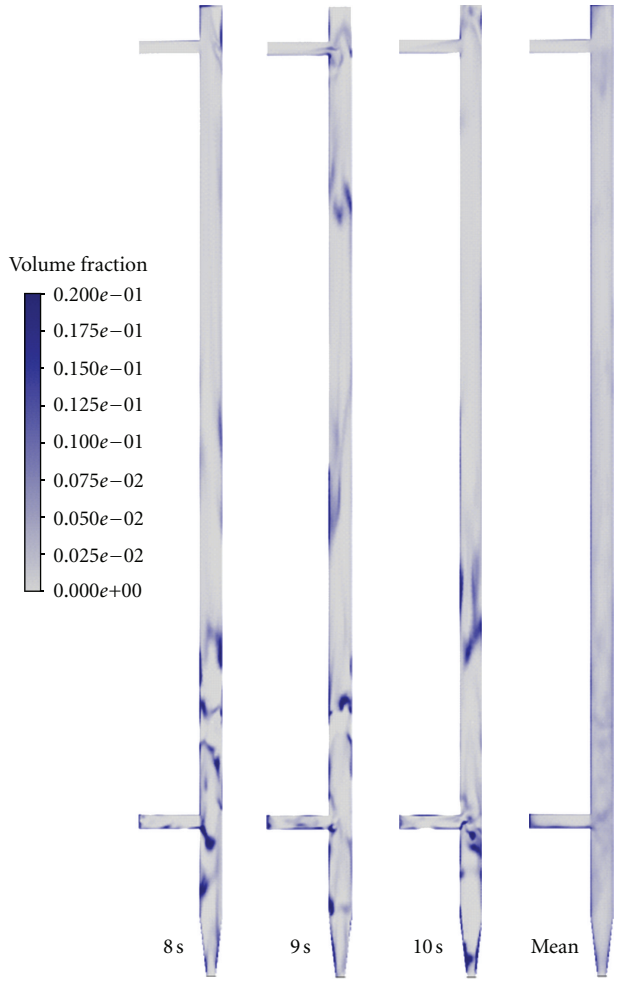

Figure 7: Instantaneous solid-phase volume fraction at 8, 9, and 10 seconds and the mean time average on an axial plane of the riser.

the semiempirical estimation, an over-predicted simulated result of 7.5%.

The oscillatory characteristic of the mass flux at the exit can be explained by the continuous disappearance and formation of clusters along the riser, which determines the solid radial distribution and the vertical displacement of particles into the column, also to be observed in Figure 7. The higher mass flux peaks occur as a consequence of this behavior. The slug frequency at the riser exit is around 0.36 Hz (2.8 s time period), as verified by the power spectrum density (PSD) analysis of solids mass flux fluctuation, shown in Figure 4(b). The frequency of the largest peak was within the same range as reported by other research works [21, 41]. This analysis was carried out with a sampling time of 0.01 s.

In Figure 5 comparison of the pressure drop with the values predicted by the CFD and semiempirical models is shown. The total pressure drop for the full height of the riser had a higher value with the semiempirical model; however, considering the region above of the solids return level, the results were similar. This behavior can be better understood by analyzing Figure 6, which shows the mean axial pressure and solid volume fraction profiles in the riser. The time-averaged volume fraction profile of Figure 6(b) was calculated on several consecutive cross-section planes along the height of the riser, according to the following expression:

$$\frac{1}{A}\int \varepsilon dA = \frac{1}{A}\sum_{i=1}^{n} \varepsilon_i |A_i|. \quad (1)$$

The CFD simulation indicates that the voidage fraction is not strongly segregated into a bottom dense region and an upper dilute one, but these regions are still clearly identified. Higher solid volume fraction zones were observed to occur close to the recirculation inlet height and at the T-shaped exit. This differs from the semiempirical model assumption of a much denser region at the bottom, a mean volume fraction of 0.1 against 0.04 from the simulation, thus explaining the lower pressure at the base of the riser.

Although the CFD model showed only a small difference between a denser region at the bottom and a more dilute above, the core-annulus behavior of the gas-solid flow found in the fast fluidization regime was verified. This configuration is commonly found in fast fluidization gas-solid flow in risers [19]. In this pattern a dilute core flows

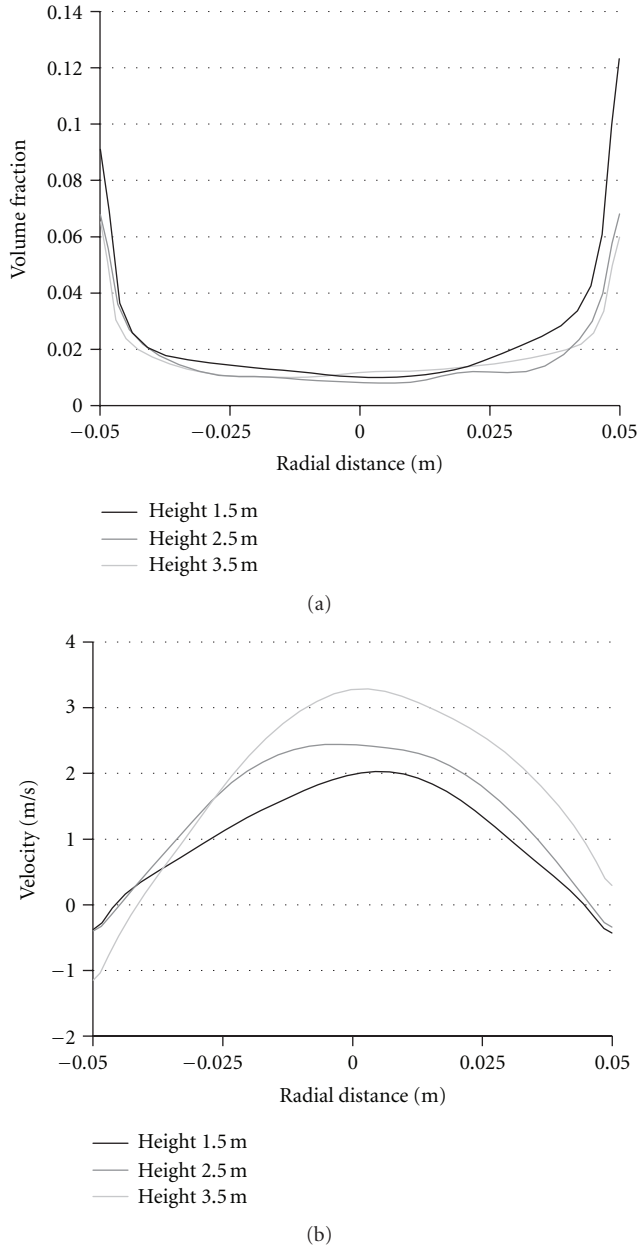

Figure 8: CFD simulation solid phase mean radial profiles of (a) volume fraction; (b) axial velocity component at 1.5 m, 2.5 m, and 3.5 m.

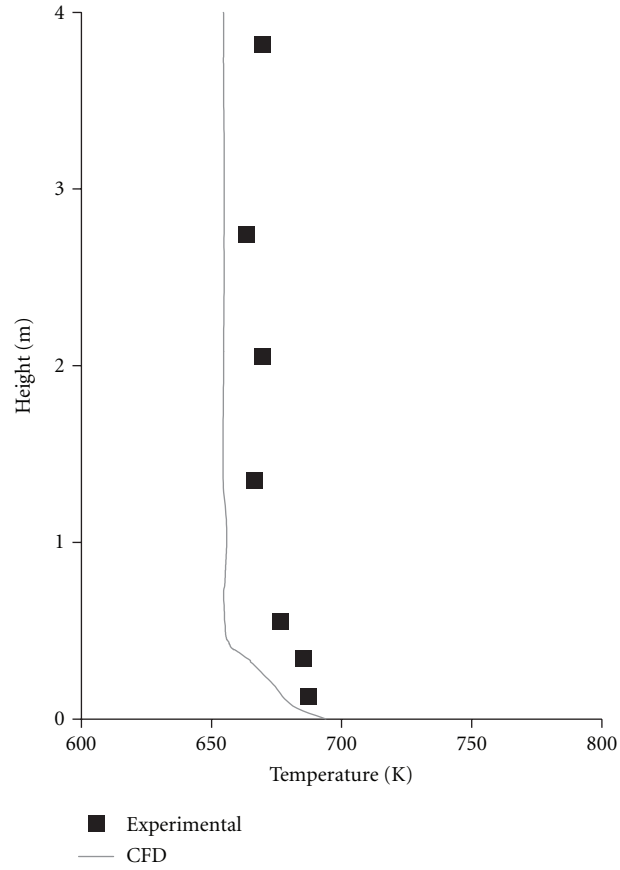

Figure 9: Time-averaged gas phase temperature profile at the axial central position in the riser compared with the experimental data.

upwards and a denser ring falls near the walls. The core-annulus is more accentuated in the upper-half region of the riser, where the influence of the recirculation entry is less intense. This tendency is also observed at the column base where the riser's diameter decreases to prevent the solids from falling further down and out off the loop, Figure 7.

Karri and Knowlton [42] remarked that the annulus structure can move cocurrently or countercurrently depending on the gas velocity and particulate flow rate. In Figure 8 the velocity and volume fractions profiles of the solid phase at three different positions in the riser are shown. A mostly counter-current pattern was identified, indicating internal recirculation. This characteristic helps to build a more uniform temperature profile along the height of the riser, as vertical mixing of the particulate phase occurs.

Furthermore, the thermal behavior of the gas-solid flow along the riser was analyzed. Figure 9 provides the gas phase temperature profile in the axial direction, showing reasonable agreement with the experimental data.

As described previously, fluidizing gas heated in a GLP burner is introduced by the main inlet flow. The system loses thermal energy through the walls and by heating the solids returning to the system through the L-valve. To account for the heat loss, the heat flux at the wall was estimated considering only the external natural convection for a vertical cylinder with a constant mean external wall temperature of 338 K and an atmospheric temperature of 303 K. The total amount of heat lost to the environment under this condition was around 175 W/m^2, which was set as the thermal boundary condition at the walls. This approximation was considered more realistic than an adiabatic wall. From the base of the riser to the lateral inlet, a temperature reduction was observed due to the return of the recirculated particles and the injection of auxiliary gas. In that region, the simulated results showed some deviation from the experimental measurement. However, the difference was lower than 22 K for the second and third

points. Above that region, where the flow is more developed, a better agreement was found.

5. Conclusions

A practical semiempirical model based on hydrodynamic correlations from experimental data was proposed for determination of the main characteristics of a bench-scale CFB unit. This model predicts the solids inventory in components of the system, thereby providing important information for more detailed simulations through a CFD approach. The semiempirical model was validated with experimental information obtained from a bench-scale CFB unit operating under precombustion conditions. Deviation for key operational parameters, such as superficial gas velocity, solids inventory, and aeration mass flow rate in the recirculating valve were below 30%.

CFD simulations of the riser of the CFB unit were also carried out. In these simulations the realizable k-epsilon model described the turbulence of the continuous phase and the KTGF was applied to the description of the dispersed phase flow in the two-fluid model of the riser section of the CFB. The hydrodynamics verified the core-annulus model, which is also confirmed by most of the studies found in literature on fast fluidization beds. The solid circulation rate showed good agreement with the semiempirical model predictions. The simulated thermal profile in the riser showed small underpredicted values with respect to the experimental data, not larger then 3%.

The study also showed the viability of applying the semiempirical correlations to determine the solids inventory as an initial condition to a CFD simulation. By this approach less computational time is required to attain the pseudo-steady state than it would be to initialize the same simulation with an empty riser and constant G_s. Because the semiempirical model was based on operational data of several CFB units, some deviation will always be found in the values predicted for a specific unit. Nevertheless, in the absence of experimental information, the approach presented in this paper can be a useful alternative approximation.

Nomenclature

a: Decay constant
A: Area, m^2
Ar: Archimedes number
C: Solid-to-gas mass ratio at the entrance of the cyclone
Cd: Drag coefficient
d, D: Diameter, m
f: Friction coefficient
g: Gravity, m/s^2
g_0: Radial distribution
G: Circulation mass flux, $kg/m^2.s$
h: Height of the secondary air injection, m
H: Total height of the riser, m
I: Inventory, kg
k: Thermal conductivity, W/m.K
K: Model factor
L: Length, m
m: Mass rate, kg/h
Nu: Nusselt number
P: Pressure, Pa
R: Internal recirculation rate
Re: Reynolds number
t: Time, s
T: Temperature, K
u, U Velocity, m/s
v: Velocity, m/s
V: Volume, m^3.

Greek Letters

α_1: Model parameter
β_1: Model parameter
β: Interphase momentum exchange coefficient, $kg/m^3 \cdot s$
ε: Volume fraction
ϕ: Sphericity
λ: Solid bulk viscosity, $P \cdot s$
μ: Shear viscosity, $Pa \cdot s$
θ: Granular temperature, m^2/s^2
ρ: Density, kg/m^3
σ: Shear stress, Pa
v: Velocity, m/s
τ: Stress tensor, Pa
T: Solid stress tensor, Pa.

Subscripts

c: Cyclone
ch: Choking
e: Entry
f: Falling
g: Gas phase
i: Phase index
lv: L-valve
mf: Minimum fluidization
ns: Nonspherical
o: Outlet
r: Riser
s: Solid phase
sp: Standpipe
sr: Solids return level
t: Terminal
tr: Transport
w: Wall.

Acknowledgment

This work was supported by the national agency CNPq.

References

[1] E. Hartge, Y. Li, and J. Werther, "Flow structure in fast fluidized beds," in *Fluidization V*, K. Ostergaard and A. Sorensen, Eds., pp. 345–352, Engineering Foundation, New York, NY, USA, 1986.

[2] P. Basu, *Combustion and Gasification in Fluidized Beds*, Taylor & Francis, Boca Raton, Fla, USA, 2006.

[3] T. Knowlton, "Nonmechanical solids feed and recycle devices for circulating fluidized beds," in *Circulating Fluidized Bed Technology II*, P. Basu and J. Large, Eds., pp. 31–41, Pergamon Press, Oxford, UK, 1988.

[4] X. Wang, M. Rhodes, and B. Gibbs, "Solids flux distribution in a CFB riser operating at elevated temperatures," in *Fluidization VIII*, F. Large and C. Laguérie, Eds., pp. 236–244, Engineering Foundation, New York, NY, USA, 1996.

[5] J. F. Davidson, "Circulating fluidised bed hydrodynamics," *Powder Technology*, vol. 113, no. 3, pp. 249–260, 2000.

[6] H. Tong, H. Li, X. Lu, and Q. Zheng, "Hydrodynamic modeling of the L-valve," *Powder Technology*, vol. 129, no. 1–3, pp. 8–14, 2003.

[7] A. Gungor and N. Eskin, "Effects of operational parameters on emission performance and combustion efficiency in small-scale CFBCs," *Journal of the Chinese Institute of Chemical Engineers*, vol. 39, no. 6, pp. 541–556, 2008.

[8] M. J. Rhodes and P. Laussmann, "Study of the pressure balance around the loop of a circulating fluidized bed," *Canadian Journal of Chemical Engineering*, vol. 70, no. 4, pp. 625–630, 1992.

[9] M. L. Mastellone and U. Aren, "The effect of particle size and density on solids distribution along the riser of a circulating fluidized bed," *Chemical Engineering Science*, vol. 54, no. 22, pp. 5383–5391, 1999.

[10] S. W. Kim and S. D. Kim, "Effects of particle properties on solids recycle in loop-seal of a circulating fluidized bed," *Powder Technology*, vol. 124, no. 1-2, pp. 76–84, 2002.

[11] X. Qi, J. Zhu, and W. Huang, "Hydrodynamic similarity in circulating fluidized bed risers," *Chemical Engineering Science*, vol. 63, no. 23, pp. 5613–5625, 2008.

[12] Y. Chong, D. O'Dea, L. Leung, and D. Nicklin, "Design of standpipe and non-mechanical V-valve for a circulating fluidized bed," in *Circulating Fluidized Bed Technology II*, P. Basu and J. Large, Eds., pp. 493–500, Pergamon Press, Oxford, UK, 1988.

[13] X. L. Yin, C. Z. Wu, S. P. Zheng, and Y. Chen, "Design and operation of a CFB gasification and power generation system for rice husk," *Biomass and Bioenergy*, vol. 23, no. 3, pp. 181–187, 2002.

[14] R. Dewil, J. Baeyens, and B. Caerts, "CFB cyclones at high temperature: operational results and design assessment," *Particuology*, vol. 6, no. 3, pp. 149–156, 2008.

[15] G. C. Lopes, L. M. Rosa, M. Mori, J. R. Nunhez, and W. P. Martignoni, "Three-dimensional modeling of fluid catalytic cracking industrial riser flow and reactions," *Computers and Chemical Engineering*, vol. 35, pp. 2159–2168, 2011.

[16] L. Yu, J. Lu, X. Zhang, and S. Zhang, "Numerical simulation of the bubbling fluidized bed coal gasification by the kinetic theory of granular flow (KTGF)," *Fuel*, vol. 86, no. 5-6, pp. 722–734, 2007.

[17] D. Gidaspow, *Multiphase Flow and Fluidization*, Academic Press, London, UK, 1994.

[18] B. G. M. van Wachen, *Derivation, implementation and validation of computer simulation models for gas-solid fluidized beds [Ph.D. thesis]*, Delft University, 1998.

[19] S. Benyahia, M. Syamlal, and T. J. O'Brien, "Particle Technology and Fluidization. Study of the ability of multiphase continuum models to predict core-annulus flow," *AIChE Journal*, vol. 53, no. 10, pp. 2549–2568, 2007.

[20] J. C. S. C. Bastos, L. M. Rosa, M. Mori, F. Marini, and W. P. Martignoni, "Modelling and simulation of a gas-solids dispersion flow in a high-flux circulating fluidized bed (HFCFB) riser," *Catalysis Today*, vol. 130, no. 2–4, pp. 462–470, 2008.

[21] V. Jiradilok, D. Gidaspow, S. Damronglerd, W. J. Koves, and R. Mostofi, "Kinetic theory based CFD simulation of turbulent fluidization of FCC particles in a riser," *Chemical Engineering Science*, vol. 61, no. 17, pp. 5544–5559, 2006.

[22] X. Lan, C. Xu, G. Wang, L. Wu, and J. Gao, "CFD modeling of gas-solid flow and cracking reaction in two-stage riser FCC reactors," *Chemical Engineering Science*, vol. 64, no. 17, pp. 3847–3858, 2009.

[23] X. Wang, B. Jin, W. Zhong, and R. Xiao, "Modeling on the hydrodynamics of a high-flux circulating fluidized bed with geldart group a particles by kinetic theory of granular flow," *Energy and Fuels*, vol. 24, no. 2, pp. 1242–1259, 2010.

[24] A. Samuelsberg and B. H. Hjertager, "An experimental and numerical study of flow patterns in a circulating fluidized bed reactor," *International Journal of Multiphase Flow*, vol. 22, no. 3, pp. 575–591, 1996.

[25] J. J. Ramirez-Behainne, *Assessment of mercury emissions from Brazilian coal combustion in fast fluidized bed [Ph.D. thesis]*, UNICAMP, Campinas, Brazil, 2007.

[26] W. C. Yang, "Modification and re-interpretation of Geldart's classification of powders," *Powder Technology*, vol. 171, no. 2, pp. 69–74, 2007.

[27] R. I. Hory, J. J. Ramirez-Behainne, A. A. B. Pécora, and L. Goldstein Jr, "An empirical model to predict the mass flow rate of solids in a high temperature circulating fluidized bed system," in *Proceedings of the 11th Brazilian Congress of Thermal Sciences and Engineering*, ENCIT, 2006.

[28] C. Y. Wen and Y. U. Yu, "A generalized method for predicting the minimum fluidization velocity," *American Institute of Chemical Engineers Journal*, vol. 12, pp. 610–612, 1966.

[29] D. Bai, Y. Jin, and Z. Yu, "Flow regimes in circulating fluidized beds," *Chemical Engineering and Technology*, vol. 16, no. 5, pp. 307–313, 1993.

[30] D. Kunii and O. Levenspiel, "Entrainment of solids from fluidized beds I. Hold-up of solids in the freeboard II. Operation of fast fluidized beds," *Powder Technology*, vol. 61, no. 2, pp. 193–206, 1990.

[31] D. Kunii and O. Levenspiel, "Flow modeling of fast fluidized beds," in *Circulating Fluidized Bed Technology III*, P. Basu, M. Hasatani, and M. Horio, Eds., pp. 91–98, Pergamon Press, Oxford, UK, 1991.

[32] W. C. Yang, "Criteria for choking in vertical pneumatic conveying lines," *Powder Technology*, vol. 35, no. 2, pp. 143–150, 1983.

[33] J. Perales, T. Coll, M. Llop, L. Puigjaner, J. Arnaldos, and J. Casal, "On the transition from bubbling to fast fluidization regimes," in *Circulating Fluidized Bed Technology III*, P. Basu, M. Hasatani, and M. Horio, Eds., pp. 73–78, Pergamon Press, Oxford, UK, 1991.

[34] J. J. Ramirez-Behainne and G. Martins, "A semi-empirical model to calculate the inert solid inventory and the main dimensions of a CFB reactor aiming biomass thermochemical conversion," in *Proceedings of the 20th International Congress of Mechanical Engineering*, 2009.

[35] E. Muschelknautz and V. Greif, "Cyclone and other gas-solid separators," in *Circulating Fluidized Beds*, J. Grace, A. Avidan, and T. Knowlton, Eds., pp. 181–213, Blackie Academic & Professional, London, UK, 1997.

[36] T. Knowlton, "Standpipes and return systems," in *Circulating Fluidized Beds*, J. Grace, A. Avidan, and T. Knowlton, Eds., pp. 214–260, Blackie Academic & Professional, London, UK, 1997.

[37] D. Geldart and P. Jones, "The behaviour of L-valves with granular powders," *Powder Technology*, vol. 67, no. 2, pp. 163–174, 1991.

[38] S. Ogawa, A. Umemura, and N. Oshima, "On the equations of fully fluidized granular materials," *Journal of Applied Mathematics and Physics*, vol. 31, no. 4, pp. 483–493, 1980.

[39] C. K. K. Lun, S. B. Savage, D. J. Jeffrey, and N. Chepurniy, "Kinetic theories for granular flow: inelastic particles in Couette flow and slightly inelastic particles in a general flowfield," *Journal of Fluid Mechanics*, vol. 140, pp. 223–256, 1984.

[40] W. E. Ranz and W. R. Marshall Jr., "Evaporation and drops—part I and II," *Chemical Engineering Prog*, vol. 48, pp. 173–180, 1952.

[41] S. Benyahia, H. Arastoopour, T. M. Knowlton, and H. Massah, "Simulation of particles and gas flow behavior in the riser section of a circulating fluidized bed using the kinetic theory approach for the particulate phase," *Powder Technology*, vol. 112, no. 1-2, pp. 24–33, 2000.

[42] S. B. R. Karri and T. M. Knowlton, "A comparison of annulus solids flow direction and radial solids mass flux profiles at low and high mass fluxes in a riser," in *Proceedings of the 6th International Conference on Circulating Fluidized Beds*, pp. 71–76, 1999.